AD_____

Award Number: W81XWH-10-1-0267

TITLE: Development of Prior Image-Based, High-Quality, Low-Dose Kilovoltage Cone Beam CT for Use in Adaptive Radiotherapy of Prostate Cancer

PRINCIPAL INVESTIGATOR: Xiao Han

CONTRACTING ORGANIZATION: THE UNIVERSITY OF CHICAGO
CHICAGO, IL 60637

REPORT DATE: May 2013

TYPE OF REPORT: Annual Summary

PREPARED FOR: U.S. Army Medical Research and Materiel Command
Fort Detrick, Maryland 21702-5012

REPORT DOCUMENTATION PAGE

Form Approved
OMB No. 0704-0188

1. REPORT DATE	2. REPORT TYPE	3. DATES COVERED
May 2013	Annual Summary	15 April 2010- 14 April 2013

4. TITLE AND SUBTITLE
Development of Prior Image-Based, High-Quality, Low-dose Kilovoltage Cone Beam CT for Use in Adaptive Radiotherapy of Prostate Cancer

5a. CONTRACT NUMBER

5b. GRANT NUMBER
W81XWH-10-1-0267

5c. PROGRAM ELEMENT NUMBER

6. AUTHOR(S)
Xiao Han

5d. PROJECT NUMBER

5e. TASK NUMBER

5f. WORK UNIT NUMBER

7. PERFORMING ORGANIZATION NAME(S) AND ADDRESS(ES)
The University of Chicago
Chicago, IL 60637-5418

8. PERFORMING ORGANIZATION REPORT NUMBER

9. SPONSORING / MONITORING AGENCY NAME(S) AND ADDRESS(ES)
U.S. Army Medical Research and Materiel Command
Fort Detrick, Maryland 21702-5012

10. SPONSOR/MONITOR'S ACRONYM(S)

11. SPONSOR/MONITOR'S REPORT NUMBER(S)

12. DISTRIBUTION / AVAILABILITY STATEMENT
Approved for Public Release; Distribution Unlimited

13. SUPPLEMENTARY NOTES
Cone-beam Computed Tomography, Adaptive Radiation Therapy, Radiation Dose

14. ABSTRACT

Adaptive radiotherapy (RT) is an advanced technique for prostate cancer treatment which employs kilovoltage (KV) cone-beam CT (CBCT) for guiding treatment. High quality CBCT images are important in achieving improved treatment effect, but they also require a non-negligible amount of imaging radiation dose which raises patient safety concern. Therefore, the goal of this project is to investigate and develop innovative, prior-image-based CBCT imaging techniques that can yield high quality images with reduced dose. Throughout the three years of this project, I have conducted research tasks as planned. I have investigated and developed prior-image-based, narrowly collimated KV CBCT imaging configurations, have developed prior-image-based, few-view CBCT image-reconstruction algorithms, and have validated and evaluated the proposed configurations and algorithms. I have achieved the goals planned for this project. The techniques developed can potentially improve current CBCT image quality, and can enable novel, high-quality, low-dose CBCT imaging configurations.

15. SUBJECT TERMS-

16. SECURITY CLASSIFICATION OF:			17. LIMITATION OF ABSTRACT	18. NUMBER OF PAGES	19a. NAME OF RESPONSIBLE PERSON
a. REPORT	b. ABSTRACT	c. THIS PAGE			USAMRMC
U	U	U	UU		19b. TELEPHONE NUMBER *(include area code)*

Table of Contents

	Page
Introduction……..	**5**
Body……..	**6**
Key Research Accomplishments……..	**23**
Reportable Outcomes……	**24**
Conclusion……	**30**
References……	**31**

INTRODUCTION

Prostate cancer is the most common non-skin cancer and the second leading cause of cancer death among American men [1]. Modern radiotherapy of prostate cancer relies heavily on imaging technologies for accurate patient setup and target localization [2]. In adaptive RT[3], one of the most advanced RT techniques, the treatment plan is adaptively adjusted according to the tumor's change in position, size, and shape [4-6]. Therefore, high-quality 3D images with good soft-tissue contrast are necessary for achieving successful adaptive RT. Kilovoltage CBCT has shown its capability of yielding such images to guide the prostate cancer treatment [7-8]. However, frequent use of high quality CBCT images is often associated with a substantial amount of imaging radiation dose [9-12], which raises concerns about patient safety. On the other hand, one unique feature of clinical CBCT is the availability of a high-quality diagnostic CT image, which can be incorporated in the CBCT image reconstruction as prior knowledge. The objective of this project is to investigate and develop advanced CBCT imaging techniques that utilize prior images for optimized image quality and reduced imaging dose.

Throughout the three years of this project, my effort has been supported by a Predoctoral Trainee Award, and I have conducted research tasks as planned. As discussed below, I have investigated and implemented novel scanning trajectories with aid of additional hardware components and software control. Simulation data have been generated for initial test of object coverage for these scanning trajectories. I have also acquired real data of physical phantoms by using a clinical CBCT system under a variety of sampling configurations, including full-view, sparse-view, truncated data, and offset-detector configurations. I carried out a rigorous investigation on developing optimization-based image reconstruction algorithms by specifying a discrete imaging model, formulating optimization programs, and designing and implementing iterative algorithms. I have designed a host of parameters for the imaging model, optimization programs, and iterative algorithms, and strategies for adaptively selecting these parameters have been laid out. I have used developed optimization-based algorithms to reconstruct images from data acquired under various sampling configurations. Prior images have been investigated for incorporation in image reconstruction tasks for all the data acquisition configurations. Physical phantoms, including standardized QA phantom and anthropomorphic phantoms, were scanned with CT and CBCT for evaluation of the algorithms developed. Patient data were collected and used for full- and few-view reconstruction. I have validated, characterized, and assessed the reconstruction quality by using simulation data, physical phantom data, and patient data. Quantitative metrics have been calculated for quantitatively characterizing and evaluating the reconstruction quality, choice of parameters, and strategies for incorporating prior images. I have demonstrated that prior-image-incorporated iterative reconstruction algorithms can potentially enhance high-quality CBCT images for IGRT, and that images such reconstructed from substantially reduced data may still bear high clinical IGRT utility.

I have achieved the goals planned for this project. The techniques developed in the project have high technical significance in that image quality of current CBCT can potentially be improved by the algorithms developed, and that novel, high-quality, low-dose CBCT imaging can be enabled by the algorithms developed.

BODY

1 Research Accomplishments

1.1 Investigate and develop novel CBCT scanning techniques

1.1.1 Implement narrow beam collimation for CBCT ROI imaging

I have designed and implemented a collimation device and integrated it to the clinical CBCT system. With the add-on device, the current system can perform ROI imaging by acquiring projection data only corresponding to the ROI. I chose to design this device to have similar shape and form factor to the current collimator used to hold the bow-tie filter for X-ray intensity profile shaping, such that additional mechanical complexity is minimized. Another advantage of this design is that mounting is straight forward, which eliminates concerns about mis-alignment with the current system geometry. I then purchased the material, cut it to fit in the enclosure, and fixed it. I then mounted the device to replace the bow-tie filter holder for achieving narrow X-ray collimation. When I finish data acquisition, the bow-tie filter can be put back for normal clinical use.

I acquired numerous narrow beam collimation cone-beam data sets under different configurations using the developed device. First, the two blocking materials were adjusted to have different separation distances for achieving varying degrees of beam collimation, which lead to different sizes of illuminated ROI. Second, I changed different materials for X-ray blocking to reduce the X-ray leakage from the blocked region. Third, I developed an improved version of the device with dynamic collimation capability, which can be used to dynamically adjust the degree of collimation during gantry rotation/data acquisition.

1.1.2 Reproduce the same imaging geometric configurations on CBCT ROI scan as those on prior diagnostic CT scan

Design of numerical and physical phantoms: I first carried out phantom design by using computer-simulation data, which we can select the shape, size, and materials of the structures embedded in a tissue-equivalent environment. I then generated raw projection data using the geometric configuration of the actual CBCT system, including the source-to-isocenter and detector-to-isocenter distances, as well as the angular information for each projection view recorded by the scanner. Furthermore, I considered major physical factors involved in CBCT imaging that deviate data from ideal line-integral projections, which include scatter, beam-hardening, and noise. On top of the raw projection data I simulated scattered X-rays using different scatter-to-primary ratio (SPR) parameters, including the simplified case of a constant profile and more complicated but also more accurate case of convolving the primary photons with a Gaussian kernel. I also obtained the actual X-ray spectrum data measured from the CBCT system under study, which I incorporated in the computer-simulation program for realistic simulation of beam-hardening effect due to the polychromatic nature of the X-ray from the linear accelerator. Furthermore, I added noise to data using a number of different noise models, including Gaussian-, Poisson-, and compound Poisson-distributed noise. I also varied the noise level to mimic different mAs used in clinical and research modes of the CBCT system.

Based upon experiences with the numerical phantom, I designed and made a physical phantom for data acquisition which have insert structures that mimic the density of human organs. I first decided to make the phantom to have similar size to a human head to avoid truncation issues

as a starting point, and plan to design and make another larger phantom to have similar size to pelvis. I then looked up the X-ray attenuation coefficients of different plastic materials that have similar attenuation coefficients to the postate, surrounding soft-tissues, as well as bones. I then obtained the materials from a vendor and assembled the phantom in a plastic enclosure to be filled with water as the background.

Prior diagnostic CT scan and geometry reproduction on CBCT ROI scan: I acquired prior images of the standard calibration phantom and the physical phantom I made using a Philips 64-slice diagnostic CT scanner that I have access to in the Radiation Oncology department. I selected different scanning protocols to acquire data sets of different quality, i.e., noise levels, etc. Though I tried different methods to reproduce the geometric configurations of the prior diagnostic scan on CBCT system, this task proved challenging, mainly for two reasons: (1) the source-to-isocenter and detector-to-isocenter distances are different for the diagnostic scanner and the CBCT scanner and those are difficult, if not impossible, to adjust. (2) the angular position of each projection view are not exactly the same, and interpolation across different views can introduce noticeable loss of spatial resolution.

1.1.3 Generate data from the prior image based upon the CBCT ROI scan configurations and obtain synthesized projection data

I decided to choose the approach of generating data from the prior image to supplement the missing portion in the CBCT ROI scan. I first reconstructed a prior image from diagnostic scan data using the standard FDK algorithm. I then estimated the size of the CBCT scan ROI in the reconstructed image space, and using this information to remove the corresponding region in the prior image. I then generated data from the prior image with only the peripheral region using a discrete forward projector. The forward projection was carried out according to the exact same geometric configurations used in the CBCT scan, i.e., the same source-to-isocenter and detector-to-isocenter distances as well as identical angular positions. I then combined the forward projected data with the CBCT ROI data to obtain a new, synthesized data set without transverse truncation which is mathematically ready for reconstruction.

1.1.4 Scatter compensation for synthesized physical phantom data

Compared to diagnostic CT where X-ray beam spanning a relatively small cone-angle is used to illuminate the object, CBCT employs X-ray beam with a much larger cone-angle which illuminates a significantly greater portion of the object/patient [7]. As such, CBCT data contain a much higher component coming from scattered photons rather than primary photons (i.e., photons impinging on the detector after penetrating through the patient along a linear trajectory). This scatter component of the data introduces deviation from and thus inconsistency with the standard X-ray transform model, and therefore must be compensated for or corrected before reconstruction is carried out. The necessity in the particular case of patient prostate localization is critical, as the subtle contrast between the prostate and surrounding soft-tissues can be easily reduced or even diminished by the scatter component having a low spatial frequency. On the other hand, accurate scatter correction is known as a difficult problem because precise knowledge about the physical process of scattering depends on the subject being scanned, and is in general unavailable prior to a CBCT scan. Nonetheless, I developed empirical compensation techniques that can produce an estimate of the scatter profile based upon the physical characteristics of scattered radiation. By appropriately adjusting parameters in the compensation technique, I could minimize the inconsis-

tency between measured data and the assumed imaging model. To verify and demonstrate the effectiveness of this technique, I compared the reconstructed images before and after performing compensation, which showed that the scatter-induced artifact can be considerably reduced.

1.1.5 Implement filtered-backprojection reconstruction from the synthesized projection data

I implemented the FDK algorithm, a standard filtered-backprojection type reconstruction algorithm, for carrying out image-reconstruction studies from data acquired and processed in previous steps. I implemented the algorithm in two different programming languages, one in IDL (ITT Visual Information Solutions, Boulder, CO) and another in C. I first wrote the code in IDL for fast debugging and test/validation purpose, and after extensive testing using standard numerical phantoms, such as Shepp-Logan phantom and FORBILD phantom [23], I implemented the C version for higher execution efficiency. Furthermore, I also implemented in each language an improved version capable of parallel-computation to utilize the multi-core CPU that I have installed on my workstation. The parallel computation of the reconstruction code written in C was implemented by use of OpenMP, and I managed to achieve an approximately 5-fold acceleration on an 8-core CPU compared to the single-thread version. I also modified the IDL code to utilize the built-in multi-threading capability provided by the newest version of the software. On one hand, because three-dimensional image reconstruction is still computationally intensive, I improved the efficiency of parallel computation by using more threads. Also I explored further improved efficiency of parallel computation enabled by a newly purchased Tesla Graphic Processing Unit (GPU, nVidia, Santa Clara, CA).

I have applied the robust and efficient FDK reconstruction implementation to reconstruct images from data synthesized with prior-image forward projection data and CBCT ROI data. The result shows promising improvement with much reduced truncation artifact.

1.1.6 Investigate and implement different imaging trajectories for CBCT

The current scanning mode of CBCT employs a circular X-ray source trajectory, i.e. the gantry rotates around the subject while the subject itself stays still. Data sampling for this source trajectory inherently limits the reconstructible region, whereas non-conventional source trajectories can potentially expand the reconstructible region. I implemented a reverse-helix trajectory for such purpose. At the time of this phase of investigation, patient couch with programmable translational motion was not available to me. Instead, I made a supporting device capable of translational motion and put it on top of the couch. During data acquisition, I programmed the translation device to feed the object along Z-axis toward the isocenter, while the gantry finishes a full 2π rotation. I then continued to feed the object along the same direction, while rotate the gantry backward for another full turn. This scanning mode accomplishes a reverse-helix source trajectory from the view-point of the object. I implemented a filtered-backprojection (FBP) plus backprojection-filtration (BPF) algorithm [14,16] to reconstruct an image from this reverse-helix data set. Results show that the region that is not reconstructible from circular trajectory data can now be reconstructed. I have designed and implemented other source trajectories including a two-circle trajectory and a line-plus-circle trajectory, which may have comparable or further enlarged reconstructible region.

1.1.7 Investigate and implement novel scanning trajectories

I have investigated and implemented non-conventional scanning trajectories for the clinical CBCT system. The current CBCT systems employ flat-panel detectors, which have limited size, and lack a slip-ring device as available on most diagnostic CT systems. Therefore, the standard circular trajectory as the only choice available on most clinical CBCT systems result in a limited axial field of view (FOV), which poses challenges in clinical applications when the CBCT images are registered to the planning CT images with a significantly larger axial coverage. Specifically, I investigated two possible solutions to extending axial coverage, a reverse-helix trajectory and a two-circle trajectory. I first investigated the theoretical axial coverage by using the Tuy's condition [13] and chord-based reconstruction theory [14]. Then, I performed test reconstructions using simulation data generated from a disk phantom and a numerical anthropomorphic phantom [15]. I also considered the implementation feasibility of these trajectories on existing systems available in radiation oncology clinic. Finally both two trajectories were implemented with aid of necessary parts and auxiliary component devices.

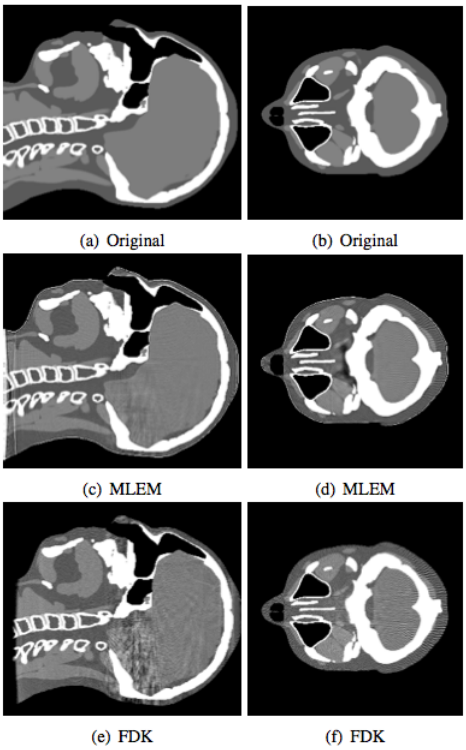

Figure 1: Images of the XCAT phantom within the middle sagittal (a, c, and e) and middle transverse (b, d, and f) slices reconstructed by use of the expectation maximization (EM, c and d) and FDK (e and f) algorithms from the two-circle scanning data. The phantom truth within corresponding slices is displayed in (a) and (b).

Reverse-helix trajectory I first investigated the reverse-helix trajectory, which has been proved to offer larger axial FOV when reconstructed by use of an innovative technique [16]. For practical feasibility, this trajectory can be realized on the clinical CBCT system with minimal additional translational feeder device and associated software control. Then, by continuously feeding in the imaged subject, while rotating the gantry two turns consecutively, first a clock-wise (CW) spin and then a counter clock-wise (CCW) spin, an effective reverse-helix trajectory was obtained. I have obtained the auxiliary devices and software and have them implemented on the clinical CBCT system.

Two-circle trajectory Compared to the reverse-helix trajectory that involves additional hardware device and software synchronization, a two-circle trajectory is more straight-forward to implement. It works by performing a full circular scan, translating the couch for a certain distance, and then performing another full circular scan. To test the extension of axial coverage, I carried out a simulated data study using numerical disk and anthropomorphic XCAT phantoms [15]. As an example, I show in Fig. 1 the reconstruction result of a two-circle scan performed with a longitudinal translation of 10 cm. The reconstruction image within the middle sagittal slice demonstrates that enlarged FOV can be achieved by use of the two-circle trajectory in combination with appropriately designed iterative algorithms.

1.2 Develop optimization-based algorithms for CBCT image reconstruction

1.2.1 Incorporation of prior images into few-view reconstruction by using partially-shifted truth image

Prior images have been incorporated into reconstruction from few-view data by using partially-shifted truth image. Specifically, I shifted the internal structures of a number of numerical phantoms, including the Shepp-Logan and FORBILD phantoms, by varying distances along different directions. While the shift was applied, the shapes and sizes of the structures were kept unchanged. In addition, I obtained realistic phantom images by retrieving CBCT images of physical phantoms and patients, and artificially introduced shifting by varying the orientation of the discretized phantom images and by translating the rotated images along three directions in the Cartesian coordinates. These shifted images have been prepared for few-view reconstruction experiments.

1.2.2 Incorporation of prior image into few-view reconstruction by using partially-deformed truth image

Prior images have been incorporated into reconstruction from few-view data by using partially-deformed truth image. I selected a set of high-contrast and a set of low-contrast structures in the Shepp-Logan and FORBILD numerical phantoms, and varied their shapes and sizes by changing their the lengths of the long- and short-axes, while keeping the rest of the phantom unchanged. In addition, from realistic phantoms obtained from CBCT images of physical phantoms and patients, I segmented out high- and low-contrast structures such as bones, markers, and soft tissues, applied deformation operations on the segmented structures, and then put them back on top of the phantom background. These modifications mimic the unavoidable internal motion of patients undergoing radiation therapy, and such modified phantom images were prepared for few-view reconstruction experiments.

1.2.3 Incorporation of prior image in few-view reconstruction

I have investigated a variety of methods for incorporating into few-view reconstruction the information of prior images, which were obtained through partially-shifted and partially-deformed truth phantom images.

Initial-guess method I have incorporated the prior images as initial-guess images in reconstruction from few-view data. Because few-view reconstruction is ill-conditioned, iterative algorithms were employed for solving the reconstruction programs. Different iterative algorithms have been developed for image reconstruction, which specify the computation procedures, while the initial starting point can theoretically be arbitrarily selected. Therefore, despite the known differences between the prior images and the images to be reconstructed from current projection data, the prior images serving as initial estimates have proved to be more effective than initial image without any prior information, such as a blank image. The results show that the higher similarity between the prior image and the current image, the less iterations it takes for iterative algorithms to converge, which is an important benefit especially for on-line CBCT imaging under strict time constraints. I have also identified the disadvantage of this method of incorporating prior image when the internal shift/deformation is significant, in which case the initial-guess did not show apparent improvement than using an arbitrary image such as a blank image with uniform values,

such as the average value of the prior image.

Local-region-update method The prior images where also incorporated into few-view reconstruction by means of the local-region-update technique. Specifically, I determined from the differences between the prior images and the current images regions that remained unchanged between scans, and explicitly incorporated this prior information as a constraint in the iterative algorithm for few-view reconstruction. The results show that, when the updating region can be accurately localized, this method is highly effective in reducing the amount of data required for reconstruction and in lowering the number of iterations needed for algorithm convergence. This is because the vast null-space associated with few-view reconstruction, which is a highly ill-conditioned problem, has been significantly reduced. On the other hand, I have found out, through numerical studies, that this technique can yield reconstruction of sub-optimal quality when the shift and deformation cover an extended region over the image support, because additional data-inconsistency can be introduced to the already ill-conditioned problem due to the unreasonably assumed localized update. Such a scenario is, however, not uncommon in practical CBCT imaging for IGRT, as the shift and deformation soft-tissue organs of patient are not satisfactorily described by a localized approximation. Therefore, the utility of this method can be limited in these scenarios due to additional image artifacts.

Image-support method I have also conducted a study on incorporating prior images by constraining the spatial support in the iterative reconstruction from few-view data. The support was estimated from the prior images for each transverse slice, which was then injected to the reconstruction as an constraint in the image domain by setting at each iteration the voxels outside of the image support to zero. Because the change of the overall image support between prior and current scans is expected to be small, a slightly dilated support than prior image can be used as a reasonable estimate. This method also demonstrated effective in reducing the null space of the ill-conditioned problem, and is less susceptible to the discrepancy between prior and current images. In particular, the support can be crucial in few-view reconstruction from truncated data, because the unmeasured portion of the subject poses challenges to estimating its extent from the current scan, leading to significantly enlarged null space. In these scenarios, the support information has shown especially important in reducing truncation-induced artifact. However, the usefulness of this technique can be limited in reducing the number of views for high-quality reconstruction, for which additional information from the prior image may need to be exploited and incorporated.

Sparsity-constraint method Based upon the observation that CBCT images of clinical IGRT interest usually have sparse representation in appropriately chosen domains, I have explored the method of incorporating sparsity information contained in the prior images. For images that have sparse representation in their native, spatial domain, the sparsity can directly be used as an additional constraint. I have developed an iterative-hard-thresholding technique for incorporating such constraints in iterative reconstruction of sparse images such as in vasculature imaging [28], where the ell_0 norm of the image was employed as a non-convex constraint in iterative reconstruction. For general images that have extended support in the spatial domain, such as CBCT images of patients in the pelvis region, the ell_0 norm is no longer a good constraint. Instead, the sparsity in the image-gradient domain was exploited for relaxing the requirement on the amount of data for reconstruction. I have adapted a TV-minimization-based reconstruction program for few-view reconstruction of CBCT images. The results show that substantial reduction of view-angles can be possible.

1.2.4 Investigate and develop the optimization-based algorithms

I have identified three key components for developing optimization-based algorithms for CBCT image reconstruction: specification and analysis of imaging model, formulation of optimization programs, and developing iterative algorithms. Each of the components involve a number of parameters, and effort has been made to developing strategies for choosing parameters appropriate to specific imaging configuration and reconstruction task.

Investigate the discrete CBCT imaging model and data divergence I have carried out detailed analysis on the imaging model of CBCT. The current image-reconstruction algorithms on clinical CBCT systems are based upon a continuous imaging model, whereas the proposed optimization-based reconstructions are derived from a discrete imaging model [20]

$$\mathbf{g_0} = \mathscr{H}\mathbf{f}, \tag{1}$$

which is distinctively different than the continuous model and has significant implications on the potential improvement on data-acquisition flexibility and image reconstruction quality. I investigated the impact of key parameters involved in the imaging model, including the basis vectors for expanding the data and image, as well as the number of pixels and voxels representing the data and image [21]. Based upon the discrete imaging model in Eq. (1), I investigated the choice of data divergence, such as the Euclidean distance or Kullback-Leibler (K-L) divergence, which are defined for quantifying the divergence between the measured data and the model data. I have determined to focus the project on Euclidean distance, because of the availability of numerous algorithms capable of efficiently reducing it. On the other hand, algorithms minimizing K-L divergence have been implemented as reference.

Optimization-program formulation Based upon the imaging model and data divergence, I have designed and investigated a variety of optimization programs for image reconstruction. Specifically, I considered various forms of image regularizations, including ℓ_0, ℓ_1, and total-variation-norms, for incorporation to the optimization programs. Among numerous optimization programs, I have identified and chosen two programs for image-reconstruction in subsequent CBCT experiments [19]:

$$\mathbf{f}^* = \text{argmin}||\mathbf{f}||_{TV} \text{ s.t. } D(\mathbf{f}) \leq \varepsilon \text{ and } f_j \geq 0, \tag{2}$$

and

$$\mathbf{f}^* = \text{argmin}||\mathbf{f}||_{TV} \text{ s.t. } D(\mathbf{f}) \leq \varepsilon, f_j \geq 0, \text{ and } ||\mathbf{f}||_0 \leq s. \tag{3}$$

The rationale for this choice is that the regularization terms effectively sparsifies the image and reduces the solution set, while iterative algorithms can readily be developed for efficiently reaching the feasible set. Either programs involve a number of parameters, such as the calculation method for image TV and choice of ε and s. I have investigated the impact of different choices for these parameters and formed strategies for making reasonable choices according to different reconstruction programs and tasks.

Iterative algorithms Optimization programs in Eqs. 2 and 3, when fully specified with a set of parameters, has each implicitly designed a solution set. Iterative algorithms then need to be employed for numerically arriving at the solution sets. To the best of my knowledge by surveying existing literature of published works, there are no standard iterative algorithms available for converging to the solution sets designed by Eqs. 2 and 3. Therefore, I have designed and implemented a number of iterative algorithms by using the adaptive-steepest-descent-POCS (ASD-POCS) [21,23] framework. The algorithms operate by alternating among several calculation steps. A POCS step is employed for reducing Euclidean distance, a steepest descent (SD) step is used for reducing image TV, and a hard-thresholding step is used for enforcing image

positivity and ℓ_0 constraint. In this process, I have accomplished a non-trivial task of selecting algorithm parameters, such that a inter-balance is struck among all the operations, and the whole algorithm approach the designed solution efficiently. Because these parameters depend upon the specific imaging configuration, imaged subject, and reconstruction task, a set of adaptive step-size adjustment scheme has been developed and implemented rather than manually interfering the parameter selection along the iterative computation.

1.2.5 Validate the optimization-based algorithms

To validate the developed optimization programs and iterative algorithms, I ran the iterative algorithms for solving their respective optimization programs from data consistent with the imaging model [22], which constitutes an ideal scenario. This is an important and necessary step for rigorous algorithm development, because an optimization program and an iterative algorithm are not expected perform well in real data situations if they fail to yield the desired solution in an ideal scenario.

Inverse-crime scenario I have carried out a numerical simulation study for validating the optimization programs and the iterative algorithms. I arranged the simulation under an "ideal" condition, where the simulated noiseless data are generated from a discrete image array using a discrete projector, and the same discrete projector is used also for backprojection during reconstruction. I refer to this well-controlled, ideal condition as an inverse-crime scenario [22], which yields a linear system with, depending on the relation between number of measurements (equations) and voxels (unknowns), one unique or an infinite number of solutions.

Validation against the designed solution The intended outcome of the iterative algorithm is the optimization program's designed solution, i.e., a solution that satisfies all its constraints. I have validated the algorithms with an inverse-crime study by using known numerical phantoms, including the Shepp-Logan and FORBILD [23] phantoms. Due to the finite number of iterations and the limited computer precision, it is challenging to evaluate mathematical convergence. Instead, I have computed metrics for each constraint of the optimization program and plotted them against the iteration number, such that the asymptotic behavior is monitored and verified.

Validation against the desired solution Once an algorithm is validated for reaching the feasible set, the reconstructed image represents a "designed solution", which I have validated by characterizing its difference against the ground truth, i.e, the original numerical phantoms, which I refer to as the "desired solution". The results show that for the algorithms under investigation, they all numerically approach, with varying efficiency, to the designed solution; and when the data are sufficient, the designed solution exhibit only numerical difference within computer precision to the desired solution.

1.2.6 Investigate the appropriate parameter control in total-variation-based image-reconstruction algorithms

Total-variation (TV) based image reconstruction algorithms can potentially yield images from much reduced data (for example, sparse-view data) without significantly compromised image quality [24,25]. Additional knowledge about the object from the prior images can provide potentially remarkable help in reducing the solution space of TV-based algorithms. However, the degree of helpfulness of the prior image also depends on the appropriate selection of algorithm parameters, which have critical impact on the path in the solution-searching process within the feasible set [28]. I investigated two such parameters, the image array size (or equivalently, the image pixel size), and the data-error tolerance parameter.

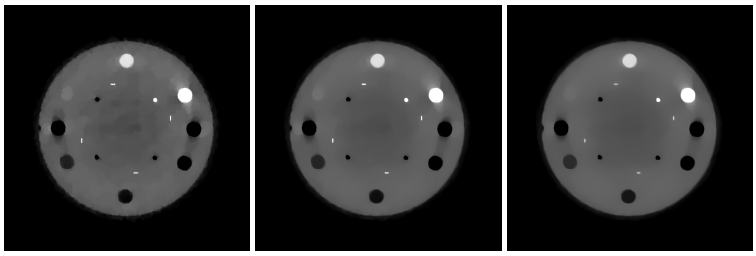

Figure 2: Images of the CATPHAN phantom within the middle transverse slice reconstructed with $\varepsilon = 8.6$ (left), 8.65 (middle), and 8.7 (right).

Choice of image array size: In TV-based image reconstruction problem the X-ray projection process is modeled as a linear system, and the dimension of the data vector is determined by the physically available elements on the detector. However, the dimension of the image vector remains a free parameter, and a different image array size mathematically defines a different linear system. Choosing a larger image array size may improve spatial resolution due to smaller pixel size, whereas the number of unknowns also increases and enlarges the feasible set, which elevates the under-determinedness of the linear system and may potentially require more projection views to avoid degradation of image quality. I have studied image reconstruction from numerical phantom and physical phantom data by using a range of pixel sizes, from those below the sampling limit (i.e. the Nyquist spatial frequency in the context of analytic reconstruction) up to four times of the limit. I found that the TV-based algorithm is capable of yielding images of satisfactory quality at over-sampled image grid, and with noise texture closer to images obtained with analytic algorithms. This result can potentially help developing reconstruction techniques that produce images of texture that observers are used to.

Choice of data-error tolerance parameter: As the main framework of the TV-based algorithms under study, we solve the following constrained minimization problem:

$$\mathbf{f}^* = \text{argmin}||\mathbf{f}||_{TV} \quad \text{s.t.} \quad |\mathscr{H}\mathbf{f} - \mathbf{g}| \leq \varepsilon \text{ and } f_j \geq 0, \tag{4}$$

where the parameter ε determines the relaxed tolerance of inconsistency between the modeled linear system and the measured data. Therefore, with other parameters fixed, each ε mathematically specifies a unique optimization problem, and, since both $|\mathscr{H}\mathbf{f} - \mathbf{g}|$ and $||\mathbf{f}||_{TV}$ are convex, a unique solution. I designed strategies to determine the range of this key parameter by carefully evaluating the degree of data inconsistency, and experimentally carried out image reconstructions with a range of ε [25]. As an example, we display in Fig. 4 images of the CATPHAN phantom reconstructed from real measurement data acquired at 120 views. With increasing ε, the images show a gradual trend of smoother appearance with a more uniform background, at the price of some low-contrast structures becoming less discernable and high-contrast objects becoming less sharp, as a trade-off.

1.2.7 Investigate reconstruction quality and data-sampling configurations

CBCT image quality can in general improve when the intensity of illuminating X-ray increase, which is also accompanied with higher imaging dose. However, given a total amount of imaging dose, there exists degree of freedoms on how to allocate the total dose to each individual projection view, on the choice of image-reconstruction algorithm, and on the selection of appropriate

algorithm parameters, all for the goal of obtaining an image that is optimal in the context of specified imaging tasks. To investigate how these variables impact image quality, I started with studying the effect of dose-allocation parameters, i.e. different combinations of view number and dose per view [19]. For this purpose I fixed the image-reconstruction algorithm as well as the associated parameters, such that the dose-allocation parameters are isolated as the only free variable.

I first carried out a simulation study using the numerical phantom. Keeping the total photon number a constant, I increased the number of views from 30 up to 720, while the number of photons per view decreases proportionally. Then from these data sets I reconstructed images using the FDK algorithm with Hanning window. I designed a set of quantitative metrics to evaluate the effect of different dose-allocation schemes on the reconstruction image quality. I then repeated the experiment using a different total photon number, which itself is a parameter and can have an impact on the results and conclusion.

I also acquired experimental CBCT data using the calibration phantom, the home-made physical phantom, and anthropomorphic phantom. To minimize data truncation, I designed and made a fixation device to avoid using the patient couch as the support. I then scanned the phantom multiple times with different settings of tube current and exposure time, such that data sets at varying mAs per view are obtained. I then obtain from the full data sets, each consists of 650 views, sparse-view data sets by extracting projection data at a subset of views that are evenly distributed over the scanning range. From these full and sparse-view data sets, I constructed data sets that have the same total mAs (i.e. mAs per view times number of views). In the end, for each of a number of total mAs values, I obtained a number of data sets with different mAs allocation schemes. From each of these data sets, I reconstructed an image using the FDK algorithm with the Hanning window.

Results of both simulation and real-data studies suggest that, when total X-ray flux is medium or high, the dose-allocation may not have a significant impact on the reconstruction quality. However, when the total X-ray flux is low, the image quality can be improved by distributing the total dose to a larger number of views.

1.2.8 Investigate the application of few-view reconstruction in imaging subjects with motion

I have studied the image reconstruction of subjects undergoing motion. Depending on the pattern of the motion, two types of motion were considered: periodic and non-periodic. For the periodic motion, I have conducted a study on reconstructing images from retrospectively sorted data. Because for a full CBCT scan, projections were only acquired for the subject at the same phase at a small number of views, the reconstruction is inherently a few-view problem. I have reconstructed images from simulated data generated at sparsely-distributed view-angles. The result shows that while the peripheral regions of the image may contain artifact due to under-sampling, the central ROI can be accurately reconstructed [24]. On the other hand, for the non-periodic motion, when the motion amplitude is small, I have designed reconstruction programs specifically for incorporating the motion. Real data of a patient undergoing contrast-agent injection and perfusion were used for the experiment. In this scenario, a prospective prediction or retrospective description of the motion trajectory may be challenging. Therefore, the data-consistency enforcement in the iterative reconstruction was relaxed to account for the small-amplitude motion. For a small subset of angular views where the motion may have a large amplitude, they were excluded from the iterative reconstruction due to the relaxed requirement on data sampling. The results show that the iterative reconstruction may be less susceptible to motion of small amplitude than conventional, analytic-based reconstructions. However, motion of large amplitude still poses a challenge for

few-view iterative reconstruction, because the excessive level of motion-induced data inconsistency.

1.2.9 Develop algorithms for reconstruction from offset-detector data

The flat-panel detectors on current CBCT systems are limited by their size, which leads to scanning field-of-views (FOV) smaller than most patient body cross-sections such as in the pelvis region. Therefore, an offset-detector geometry is employed as the clinical protocol for imaging prostate-cancer patients. Iterative reconstruction without modification yields images with artifacts manifested as a ring corresponding to the inner detector-edge due to data inconsistency, thereby preventing high-quality few-view reconstruction. I have developed an iterative algorithm that can handle offset-detector geometry by introducing a weighting matrix to both sides of the imaging model [25]. The algorithm, referred to as the adaptive-steepest-descent-weighted POCS (ASD-WPOCS) algorithm, can therefore be used for reconstruction from both standard and offset-detector geometries by using different weighting matrices.

1.3 Validate and evaluate the proposed configurations and algorithms

1.3.1 Design numerical phantoms with boney and soft-tissue structures

The algorithms developed have been tested first for their capability of achieving the solutions specified by their respective reconstruction programs. Because the reconstruction is subject-dependent, an array of numerical phantoms have been created/used for this validation purpose. Existing, well-known numerical phantoms, such as Shepp-Logan and FORBILD phantoms, were implemented according to the phantom descriptions. Additionally, a custom-made numerical phantom mimicking the human pelvis region was created by incorporating high-contrast structures such as pelvic bones and low-contrast structures such as prostate, rectum, and bladder. These boney and soft-tissue organs were modeled by ellipsoids of different shapes, and they were assigned with their corresponding attenuation coefficients. These phantoms were useful in arranging desired structures for different body cites. However, they were still considerably different than the real human body, which is of practical IGRT interest. I have found out that some results obtained with these synthetic phantoms could not translate to real phantom and patient data. Therefore, a realistic numerical phantom was obtained by casting a CT image of a patient to discrete image arrays. In this process, the CT numbers in Hounsfield Unit (HU) were converted to the linear attenuation coefficients, such that data can subsequently be generated according to X-ray path lengths. Not only did this numerical phantom include all the organs in human body, it also contained noise and other physical factors and therefore visually appear realistic. In this regard, it may contain higher value than synthetic numerical phantoms described above in mimicking practical CBCT imaging.

1.3.2 Generate phantom data simulating diagnostic scan and CBCT scans

I generated model CT and CBCT data from the numerical phantom images by performing a set of forward projections using simulated circular cone-beam scanning geometries. The phantoms were positioned on the middle plane, which is the plane containing the circular locus of the X-ray source, with their centers aligned with the center of rotation (COR). On the middle plane, the cone beam reduces to a fan beam, and the simulated curved and flat-panel detectors reduce to an arc detector and a line detector, respectively. The arc- and line-detectors were placed such that the

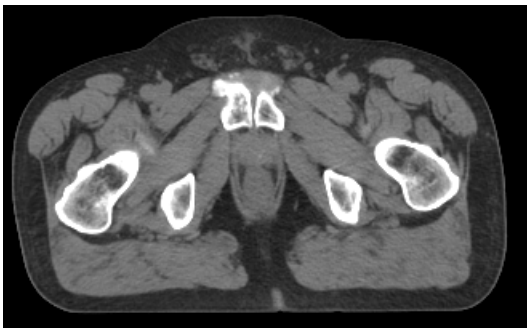

Figure 3: The numerical pelvis phantom within a transverse slice where the prostate is located.

X-ray projection of the COR intersects perpendicularly the detector at its geometric center. Other geometric parameters, such as the physical sizes of the detector pixels and the distances between X-ray sources and COR and detector planes, were assigned according to actual planning CT and on-board CBCT systems. As an example, for the pelvis phantom, each image pixel represented a physical size of 0.1 cm, and the detector was composed of 480 bins, each representing a physical size also of 0.1 cm. The source-to-COR and source-to-detector distances were 100.0 and 150.0 cm, respectively, resulting in a magnification factor of 1.5. For numerical computation purposes, some of the simulated scanning geometry was scaled down in accordance to the down-sampled phantom images.

The simulated data were generated by applying the system matrix $\mathscr{H}$ to the phantom image. Numerically, H_{ij}, the element of $\mathscr{H}$ with indexes i and j, corresponds to the contribution weight of the j-th image-pixel to the ray-sum collected at the i-th detector-bin. Under the scanning geometries specified, an X-ray does not necessarily traverse the center of an image pixel, and neither does it intersect at the center of a detector bin. Therefore, I employed a ray-driven technique for calculating H_{ij} for each ray-sum incrementally [30], and bi-linear interpolation was used for determining the contributions from multiple pixels to a ray-sum.

1.3.3 Reconstruct images using proposed algorithms from simulation data

I employed the ASD-POCS algorithm [20,21] for reconstructing images from the simulated data. Under the inverse-crime condition, the system matrix $\mathscr{H}$ used for generating data was also used for image reconstruction. In this sense, the simulated "measurement" data are identical to the model data, therefore free of inconsistency. The ASD-POCS reconstruction requires explicit specification of the data-fidelity parameter ε. While ε generally takes a positive value for image reconstruction from data containing inconsistency such as noise, the inverse-crime scenario employs model data reconstruction which is perfectly consistent with the imaging model. Therefore, ε should, in theory, be set as zero. However, because of limited computer precision, and because of the finite number of iterations used, $\varepsilon = 0$ cannot be reached practically. Moreover, the convergence metric $c_\alpha(\mathbf{f})$ becomes undefined when $\varepsilon = 0$ because the data-divergence gradient vector becomes a zero vector [19], and it cannot be employed for monitoring the algorithm convergence at $\varepsilon = 0$. Instead, in the inverse-crime studies, we selected small, but finite values for ε. Specifically, for the Shepp-Logan phantom, I have selected $\varepsilon = 1.58 \times 10^{-9}$, which is close to the numerical precision. As for the pelvis phantom, the high complexity of the image demands a prohibitively large number of iterations to converge the Euclidean divergence to an ε close to

numerical precision. Therefore, I employed an asymptotic approach to infer the behavior of the algorithm when $\varepsilon = 0$ by setting up multiple reconstructions with a descending series of ε. In the study, I selected $\varepsilon_1 = 2.4 \times 10^{-5}$, $\varepsilon_1 = 2.4 \times 10^{-6}$, and $\varepsilon_3 = 2.4 \times 10^{-7}$, and used a set of metrics to monitor the algorithm convergence.

1.3.4 Evaluate reconstructed image quality and determine configurations and algorithms for further real-data evaluation

I first performed reconstruction of the Shepp-Logan and FORBILD phantoms by using the ASD-POCS algorithm. Because these phantoms have relatively simple structures, an ε close to numerical precision was selected, and the algorithm reached convergence within about 200 iterations. The reconstructed images were visually indistinguishable from the truth images, with numerical differences, measured by root-mean-squared-error (RMSE) under 10^{-10}. I then reconstructed images of the pelvis phantom from simulated data. Due to the complex phantom structure, selection of ε near the numerical precision requires prohibitively long computation time. Therefore, by selecting a descending series of ε above numerical precision, as described above, I observed also a descending trend of reconstruction accuracy. For the smallest ε considered, the reconstruction is visually indistinguishable from the truth. The results suggest that the configurations employed in the simulation studies are likely to be adequate for real-data studies, which are available on clinical CT and CBCT systems. Moreover, the strategies for selection of algorithm parameters can be translated to real-data studies, where an additional consideration on data inconsistency will be included.

1.3.5 Acquire real data using diagnostic CT, narrow-beam CBCT, and few-view CBCT from physical phantoms

I have collected experimental data of the Catphan phantom, a Rando head phantom, and a pelvis phantom, by using CT and CBCT systems.

Data of the Catphan phantom (Model No. 504, The Phantom Laboratory, Salem, NY) were obtained by use of the OBI system with a circular cone-beam geometry on three sections: CTP515, CTP528, and CTP404. During phantom setup, we first aligned the middle plane of the CTP404 section with aid of the wire ramps, following the method suggested by the phantom manufacturer. The data obtained contain cone-beam effect, because a large volume of the phantom was irradiated. To obtain narrow-beam CBCT data, I closed the collimating blades, and only a fan-shaped region was illuminated. Two clinical scanning configurations, the high-quality head and low-dose head protocols, were adopted for data acquisition. In an attempt to investigate the impact of scanning range and angular sampling density, additional scanning configurations were also considered. In addition, the same Catphan phantom was also scanned with a planning CT under helical mode, and the reconstructed images were retrieved as prior images.

Similarly, CBCT and CT data were also acquired from a Rando head phantom, which is made of a human skull embedded in an epoxy material. Moreover, a physical pelvis phantom containing both pelvic bones and soft-tissue-mimicking materials was scanned with CT and the CBCT system on a SPECT-CT scanner.

All the acquired CBCT data were pre-processed for correcting physical factors, such as scatter, beam-hardening, and detector-response non-uniformity. These CBCT data were made ready for full- and few-view reconstruction studies, with the CT images made ready as prior images.

1.3.6 Reconstruct image using proposed algorithms with prior image-incorporated real phantom data

I have reconstructed images from real phantom data by using iterative algorithms. A variety of strategies of incorporating prior images, described in detail previously, were implemented in the reconstruction. In particular, the image-support and sparsity-constraint methods were implemented without enforcing too strong constraints, yet capable of significantly reducing the null space. On the iterative algorithm side, methods for reconstructing images onto non-isotropic voxels were developed [30], because CBCT images in clinical applications are frequently represented by voxels with axial sizes larger than transverse sizes. Also, I have adopted the strategies of selecting ε developed and refined from simulation studies to real data reconstructions. Specifically, the value of ε can either be estimated from prior images, or it can be determined adaptively in the CBCT reconstruction. In the latter case, I have selected ε as, for example, the Euclidean data-divergence reached at a certain iteration. The specific iteration number for this selection depends on the particular type of subject as well as on the scanning configuration, such as the signal-to-noise ratio (SNR) in the measurement data.

1.3.7 Evaluate and optimize image reconstruction using few-view data from physical phantom data

Evaluation studies [31] have been conducted in multiple levels throughout the project. First, the validation study with numerical phantoms described above served the purpose of evaluation of the algorithm's capability of reaching the solutions to the reconstruction program formulated. Second, I characterized the spatial resolution and contrast resolution of the Catphan phantom images by using the standardized methods routinely performed in clinical quality assurance procedures. The catphan phantom reconstructions are displayed in Fig. 4, and the spatial resolution as a function of the parameter ε is plotted in Fig. 5.

In addition, I also performed visualization-based characterization of the Rando head phantom images [31]. From the images displayed in Fig. 6, it can be observed that the iterative reconstruction yielded images of simultaneous higher spatial resolution and lower background noise.

Finally, the pelvis phantom images were reconstructed [29] and displayed in Fig. 7, from which one can see that the ASD-POCS algorithm yielded images of quality better than other algorithms.

1.3.8 Evaluate image reconstruction quality from patient data

In addition, raw projection data of a prostate-cancer patient were retrospectively collected under an Internal Review Board (IRB) approved protocol. Unlike the Rando head phantom, the pelvic region of the patient is larger than the FOV of the full-fan geometry. Therefore, the data were acquired with the low-dose thorax (LDT) protocol, a protocol employing the half-fan geometry, offered on the OBI system.

I reconstructed images from both full- and half-view patient data, and display results in Fig. 8. It can be observed that the full-view ASD-POCS reconstruction shows better delineation of the prostate than the FDK counterpart. In addition, the ASD-POCS reconstruction from half-view data appear comparable to the full-view reconstruction, suggesting minimal susceptibility to a 50% reduction of view number. By assuming that the imaging dose is linearly proportional to the number of views acquired, this translates to an effective dose reduction of 50%. However, the

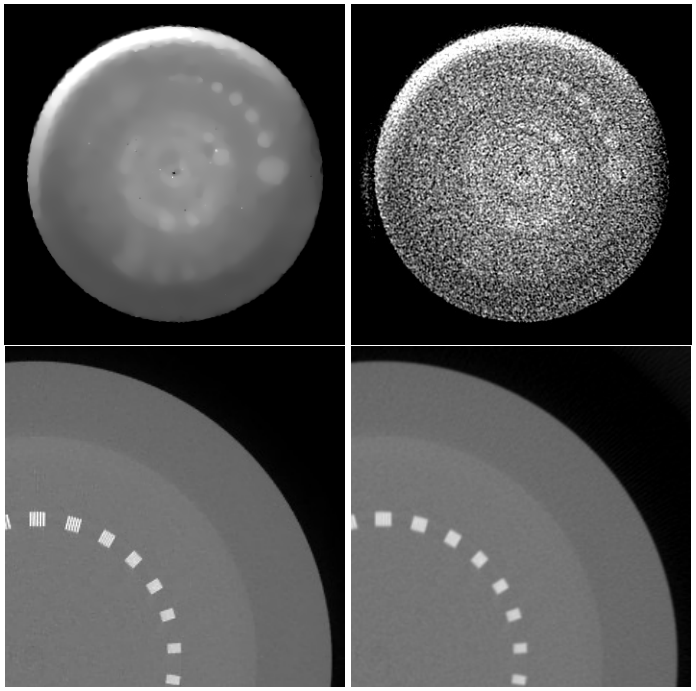

Figure 4: Images of the Catphan phantom within the CTP515 (row 1) and CTP528 (row 2) sections reconstructed by use of the ASD-POCS (column 1) and FDK (column 2) algorithms.

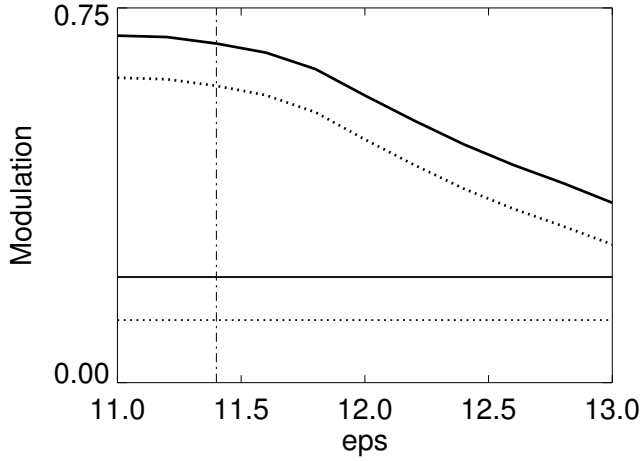

Figure 5: MTFs at 7 (solid curve) and 9 lp/cm (dotted curve) computed from CTP528 images reconstructed by use of the ASD-POCS algorithm as functions of ε. Solid and dotted horizontal lines represent the counterparts computed from FDK reference.

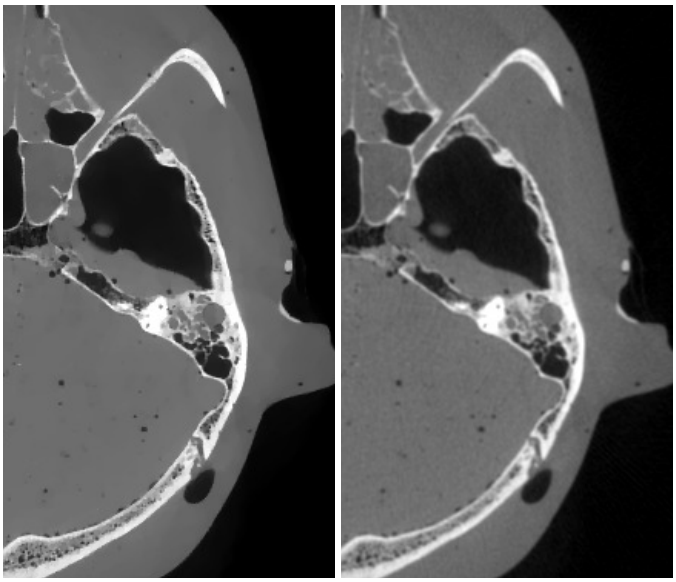

Figure 6: CBCT images of the Rando head phantom reconstructed by the ASD-POCS (left) and FDK (right) algorithms.

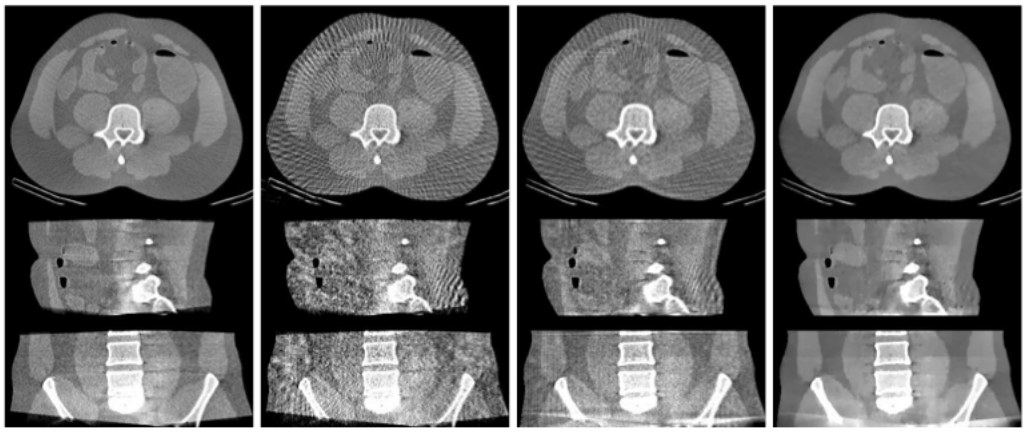

Figure 7: CBCT images of the physical pelvis phantom reconstructed from 120-view data by the FDK (column 2), EM (column 3), and ASD-POCS (column 4) algorithms. The 720-view reconstruction by FDK is displayed in column 1 as reference.

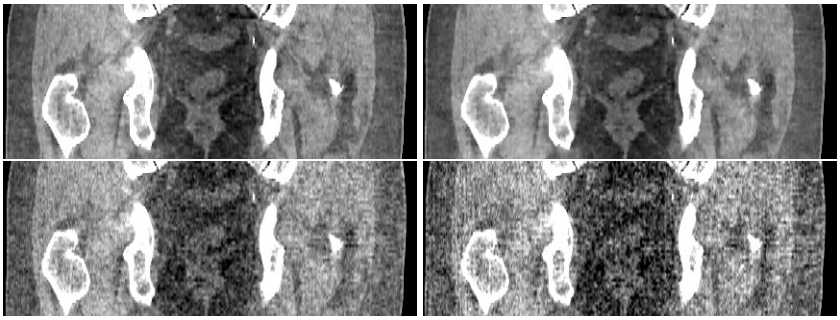

Figure 8: CBCT images of the patient within a coronal slice constructed by use of the ASD-POCS (row 1) and FDK (row 2) algorithms from the 626- and 313-view (column 2) data.

FDK algorithm is much more susceptible to the angular under-sampling, as demonstrated by the much degraded quality, especially for soft-tissue organs such as the prostate.

1.3.9 Evaluate reconstructed images with quantitative metrics

I have carried out for each simulated and real data experiment an evaluation study by calculating relevant quantitative metrics. Depending on the nature of these metrics, current effort on image-quality evaluation has been classified to similarity-metric-based evaluation and technical-efficacy-metric-based evaluation.

Similarity-metric-based evaluation I have computed quantitative metrics, including root-mean-squared error (RMSE), mutual information (MI), and universal quality index (UQI) [26] for characterizing the similarity between the designed and desired solutions. For innovative imaging configurations including sparse-view and narrow-beam illumination, the reconstructed images (i.e., designed solutions) have been compared with the images reconstructed from full-view data or data without truncation. Specifically, the impact of optimization-program parameters and algorithm parameters have been characterized by plotting these metrics versus the parameter values.

Technical-efficacy-metric-based evaluation I also computed technical-efficacy-based metrics, such as spatial resolution, contrast-noise-ratio (CNR), and detectability, for both designed and desired solutions. Due to different image texture, some metrics computed from sparse-view or truncated reconstruction can be comparable or even higher than those computed from the desired reconstruction. These metrics, however, generally decrease when the number of view decreases, or when the truncated region increases. I have therefore determined the lower bound of view reduction and upper bound of degree of truncation when the corresponding aspect of image quality falls below that computed from the desired solution.

KEY RESEARCH ACCOMPLISHMENTS

- I have implemented a collimation device and mounted it on the CBCT system for ROI data acquisition.
- I have investigated the feasibility of reproducing the geometrical configuration of diagnostic CT scan on CBCT.
- I have generated data from prior image and synthesized it with the CBCT ROI data.
- I have investigated and developed compensation techniques to reduce scatter effect.
- I have implemented filtered-backprojection algorithm for reconstructing images from synthesized projection data.
- I have investigated and implemented non-conventional imaging trajectories for CBCT.
- I have investigated optimal allocation schemes of a given total dose.
- I have investigated the effect of key parameters in TV-based algorithms.
- I have developed strategies for quantitatively evaluating quality of images reconstructed from real data.
- I have investigated and implemented reverse-helix and two-circle scanning trajectories and have obtained real data from a clinical CBCT system with these trajectories.
- I have acquired real data of physical phantom on a clinical CBCT system under full-view, sparse-view, data truncation, and offset-detector configurations.
- I have investigated and developed optimization-based algorithms for CBCT reconstruction by specifying imaging model, formulating optimization programs, and designing and implementing iterative algorithms.
- I have carried out numerical validation studies to verify the iterative algorithms for their capability of reaching the designed solution, and to verity the optimization programs for their capability of yielding designed solution close to the desired solution.
- I have reconstructed CBCT images from full-view data acquired at current clinical configurations and showed potential quality improvement by use of prior-image incorporated, optimization-based algorithms.
- I have reconstructed CBCT images from sparse-view data and showed that images comparable to what is currently used can be obtained from low-dose data containing significantly reduced projection views.
- I have reconstructed CBCT images from truncated data and showed that images comparable to what is currently used can be obtained from low-dose data containing severe truncation.
- I have reconstructed CBCT images from offset-detector data and showed that current CBCT FOV can be enlarged without introducing additional artifacts.
- I have demonstrated the efficacy of the algorithms developed by using patient data.
- I have carried out quantitative characterization and evaluation studies by calculating similarity-based and technical-efficacy-based metrics.

REPORTABLE OUTCOMES

Degree Earned

1. Doctor of Philosophy in Medical Physics, The University of Chicago, May, 2013

Peer-reviewed Journal Papers

1. **X. Han**, J. Bian, D. R. Eaker, T. L. Kline, E. Y. Sidky, E. L. Ritman, and X. Pan, "Algorithm-enabled low-dose micro-CT imaging," *IEEE Transactions on Medical Imaging*, vol. 30 (3), pp 606-620. **(Becomes one of the top five most accessed articles of *IEEE Transactions on Medical Imaging* immediately after its publication (March, 2011))**

2. J. Bian, J. H. Siewerdsen, **X. Han**, E. Y. Sidky, J. L. Prince, C. A. Pelizzari, and X. Pan,"Evaluation of sparse-view reconstruction from flat-panel-detector cone-beam CT," *Physics in Medicine and Biology*, vol. 55, pp 6575-6599, 2010. **(Featured article of *Physics in Medicine and Biology*, published online on Oct-20, 2010, one of the ten most read articles of the journal a few days after its publication until now (Feb-2011), was selected as part of the journal's highlights collection of 2010, cover story of Medicalphysicsweb Review of winter 2011, one of the ten candidates of Roberts' Prize for best paper in *Physics in Medicine and Biology* and the results will be announced in September, 2011.)**

3. D. Xia, X. Xiao, J. Bian, **X. Han**, E.Y. Sidky, F. De Carlo, and X. Pan, "Image Reconstruction from sparse data in synchrotron-radiation-based micro-tomography," *Review of Scientific Instruments* vol. 82 (4), 2011.

4. **X. Han**, J. Bian, T. L. Kline, D. R. Eaker, E. Y. Sidky, E. L. Ritman, and X. Pan, "Optimization-based reconstruction of sparse images from few-view projections," *Physics in Medicine and Biology* vol. 57 (16), 2012

5. J. Bian, J. Wang, **X. Han**, E. Y. Sidky, L. Shao and X. Pan, "Optimization-based image reconstruction from sparse-view data in offset-detector CBCT," *Physics in Medicine and Biology* vol. 58 (2), 2013

6. **X. Han**, E. Pearson, E. Y. Sidky, C. A. Pelizzari, and X. Pan, "Algorithm-enabled exploration of image-quality potential in cone-beam CT for image-guided radiation therapy," *(to be submitted in June, 2013)*

Conference Proceeding Articles

1. **X. Han**, S. Shi, J. Bian, P. Helm, E. Y. Sidky, and X. Pan, "Feasibility study of low-dose intra-operative cone-beam CT for image-guided surgery," Proc. SPIE, 7961, 79615P, 2011

2. **X. Han**, E. Pearson, J. Bian, S. Cho, E. Y. Sidky, C. A. Pelizzari, and X. Pan, "Preliminary Investigation of Dose Allocation in Low-dose Cone-beam CT," IEEE Nucl. Sci. Conf. Rec., 2010

3. **X. Han**, J. Bian, D. R. Eaker, T. L. Kline, E. Y. Sidky, E. L. Ritman, and X. Pan, "Image Reconstruction from A Reduced Number of Projections in Micro-CT Specimen Imaging," IEEE Nucl. Sci. Conf. Rec., 2010

4. **X. Han**, J. Bian, D. R. Eaker, E. Y. Sidky, E. L. Ritman, and X. Pan, "Few-view image reconstruction of coronary arteries: a preliminary study using simulation and real data," Proceedings of the First International Conference on Image Formation in X-ray Computed Tomography, 2010

5. X. Xiao, D. Xia, J. Bian, **X. Han**, E. Y. Sidky, F. De Carlo, and X. Pan, "Image reconstruction from sparse data in synchrotron-based micro-tomography of biomedical samples," Proceedings of the First International Conference on Image Formation in X-ray Computed Tomography, 2010

6. J. Bian, J. Wang, **X. Han**, E. Y. Sidky, J. Ye, L. Shao, and X. Pan, "Reconstruction from sparse data in offset-detector CBCT," Proceedings of the First International Conference on Image Formation in X-ray Computed Tomography, 2010

7. D Xia, J. Bian, **X. Han**, E. Y. Sidky, J. Lu, O. Zhou, and X. Pan, "Investigation of image reconstruction in CT with a limited number of stationary sources," Proceedings of the First International Conference on Image Formation in X-ray Computed Tomography, 2010

8. **X. Han**, J. Bian, D. R. Eaker, E. Y. Sidky, E. L. Ritman, and X. Pan, "A preliminary study of few-view image reconstruction of sparse objects in cone-beam micro-CT," Proc. SPIE, 7622-96, 2010

9. **X. Han**, S. Shi, J. Bian, P. Helm, E. Y. Sidky, and X. Pan, "Feasibility study of low-dose intra-operative cone-beam CT for image-guided surgery," Proc. SPIE, 7961, 79615P, 2011

10. Z. Zhang, J. Bian, **X. Han**, E. Pearson, E. Y. Sidky, and X. Pan,"Iterative image reconstruction with variable resolution in CT," IEEE Nucl. Sci. Conf. Rec., 2011

11. Z. Zhang, **X. Han**, J. Bian, J. J. Manak, E. Y. Sidky, and X. Pan, "Initial experience in image reconstruction from limited-angle C-arm CBCT data," IEEE Nucl. Sci. Conf. Rec., 2011

12. J. Bian, **X. Han**, K. Yang, E. Y. Sidky, J. M. Boone, and X. Pan, "A preliminary study of image reconstruction from low-dose data in dedicated breast CT," IEEE Nucl. Sci. Conf. Rec., 2011

13. J. Bian, J. Wang, **X. Han**, E. Y. Sidky, J. Ye, S. Prevrhal, H. Liang, L. Shao, and X. Pan, "Sparse-view image reconstruction from gated cardiac data," IEEE Nucl. Sci. Conf. Rec., 2011

14. J. Bian, **X. Han**, K. Yang, E. Y. Sidky, J. M. Boone, and X. Pan, "A Preliminary Investigation of Reduced-view Image Reconstruction from Low-dose Breast CT data," Proc. SPIE 8313, 831325, 2012

15. Z. Zhang, **X. Han**, J. Bian, D. Shi, A. Zamyatin, P. Rogalla, E. Sidky, and X. Pan, "Constrained TV-Minimization Image Reconstruction from Sparse-View Diagnostic CT Data," IEEE Nucl. Sci. Conf. Rec., 2012, M17-23

16. Z. Zhang, J. Bian, **X. Han**, D. Shi, A. Zamyatin, E. Y. Sidky, and X. Pan, "A Preliminary Investigation of Image Reconstruction with Variable Resolution in Diagnostic CT," IEEE Nucl. Sci. Conf. Rec., 2012, M17-22

17. J. Bian, J. Wang, **X. Han**, E. Y. Sidky, L. Shao, and X. Pan, "A Preliminary Investigation of CT-Dose Reduction for SPECT/CBCT Attenuation Correction," IEEE Nucl. Sci. Conf. Rec., 2012

18. Z. Zhang, J. Bian, **X. Han**, D. Shi, A. Zamyatin, P. Rogalla, E. Y. Sidky, and X. Pan, "Iterative Image Reconstruction with Variable Resolution in Diagnostic CT," Proceedings of the 2nd International Conference on Image Formation in X-ray Computed Tomography, 2012

19. J. Bian, K. Yang, **X. Han**, E. Y. Sidky, J. M. Boone, and X. Pan, "Constrained TV-minimization reconstruction in low-dose breast CT," Proceedings of the 12th International Meeting on Fully 3D Image Reconstruction in Radiology and Nuclear Medicine, 2013

20. Z. Zhang, J. Bian, **X. Han**, J. J. Manak, E. Y. Sidky, and X. Pan, "Optimization-based Image Reconstruction with Variable Resolutions for Cerebral Ventricle Study with C-arm Cone-beam CT", Proceedings of the 12th International Meeting on Fully 3D Image Reconstruction in Radiology and Nuclear Medicine, 2013

21. **X. Han**, E. Pearson, C. A. Pelizzari, and X. Pan, "Improved CBCT image reconstruction for IGRT," Proceedings of the Twelfth International Meeting on Fully 3D Image Reconstruction in Radiology and Nuclear Medicine, 2013

22. Z. Zhang, **X. Han**, J. Bian, D. Shi, A. Zamyatin, E. Y. Sidky, and X. Pan, "Initial Experience in Constrained-TV-minimization Image Reconstruction from Diagnostic-CT Data," Proceedings of the 2nd International Conference on Image Formation in X-ray Computed Tomography, 2012

Conference Presentations and Abstracts

1. **X. Han**, J. Bian, E. Pearson, S. Cho, E. Y. Sidky, C. A. Pelizzari, and X. Pan, "Low-dose Kilo-voltage Cone-beam CT Image Reconstruction by Constrained Total-variation Minimization: Experience with Clinical Data", IEEE Medical Imaging Conference, Orlando, Florida, October 2009

2. J. Bian, **X. Han**, K. Yang, N. Packard, E. Y. Sidky, J. M. Boone, and X. Pan, "A Feasibility Study of Breast CT Imaging with Substantially Lowered Radiation Dose" IEEE Medical Imaging Conference, Orlando, Florida, October 2009

3. D. Xia, J. Bian, **X. Han**, E. Y. E., and X. Pan, "A preliminary investigation of compressive-sensing image reconstruction from flying-focal-spot CT data," IEEE Medical Imaging Conference, Orlando, Florida, October 2009

4. **X. Han**, J. Bian, S. Cho, E. Y. Sidky, E. Pearson, C. A. Pelizzari, and X. Pan, "Accurate image reconstruction from incomplete kilo-voltage cone-beam CT data in radiation therapy," AAPM, Anaheim, CA, July 2009

5. **X. Han**, E. Pearson, J. Bian, S. Cho, E. Y. Sidky, C. A. Pelizzari, and X. Pan, "Preliminary investigation of optimal imaging parameters for dose-reduction in cone-beam CT," IEEE Medical Imaging Conference, Knoxville, TN, October 2010

6. **X. Han**, E. Pearson, S. Cho, J. Bian, E. Y. Sidky, C. A. Pelizzari, and X. Pan, "Performance evaluation of TV-minimization-based image reconstruction from OBI-sparse-data," IEEE Medical Imaging Conference, Knoxville, TN, October 2010

7. **X. Han**, J. Bian, D. R. Eaker, T. L. Kline, E. Y. Sidky, E. L. Ritman, and X. Pan, "Task-specific evaluation of low-dose, high-throughput micro-CT specimen imaging," IEEE Medical Imaging Conference, Knoxville, TN, October 2010

8. J. Bian, **X. Han**, E. Y. Sidky, J. H. Siewerdsen, and X. Pan, "Investigation of low-contrast tumor detection in algorithm-enabled low-dose CBCT", IEEE Medical Imaging Conference, Knoxville, TN, October 2010

9. J. Bian, **X Han**, J. Wang, E. Y. Sidky, L. X. Shao, and X. Pan, "Preliminary experience in sparse-view reconstruction from clinical patient data in offset-detector CBCT," IEEE Medical Imaging Conference, Knoxville, TN, October 2010

10. X. Xiao, D. Xia, J. Bian, **X. Han**, E. Y. Sidky, F. De Carlo, and X. Pan, "Image reconstruction from highly sparse data in fast synchrotron-based imaging," SPIE Optical Engineering, San Diego, California, August 2010

11. **X. Han**, E. Pearson, J. Bian, S. Cho, E. Y. Sidky, C. A. Pelizzari, and X. Pan, "Preliminary performance evaluation of CBCT Image reconstruction from reduced projection data by TV-minimization," AAPM, Philadelphia, PA, July 2010

12. **X. Han**, J. Bian, D. R. Eaker, E. Y. Sidky, E. L. Ritman, and X. Pan, "Few-view image reconstruction of coronary arteries: a preliminary study using simulation and real data," The First International Meeting on Image Formation in X-Ray Computed Tomography, Salt Lake City, UT, June 2010

13. X. Xiao, D. Xia, J. Bian, **X. Han**, E. Y. Sidky, F. De Carlo, and X. Pan, "Image reconstruction from highly sparse data of fast synchrotron-based micro-tomography of biomedical samples," The First International Meeting on Image Formation in X-Ray Computed Tomography, Salt Lake City, UT, June 2010

14. D. Xia, J. Bian, **X. Han**, E. Y. Sidky, J. Lu, O. Zhou, and X. Pan, "Investigation of image reconstruction in CT with a limited number of stationary sources," The First International Meeting on Image Formation in X-Ray Computed Tomography, Salt Lake City, UT, June 2010

15. **X. Han**, J. Bian, D. R. Eaker, E. Y. Sidky, E. L. Ritman, and X. Pan, "Sparse object reconstruction from a small number of projections in cone-beam micro-CT by constrained, total-variation minimization," SPIE Medical Imaging, San Diego, CA, February 2010

16. **X. Han**, E. Pearson, J. Bian, S. Cho, E. Y. Sidky, C. A. Pelizzari, and X. Pan, "Toward High-quality, Low-dose Cone-beam CT for Image-guided Radiation Therapy of Prostate Cancer," Innovative Minds in Prostate Cancer Today (IMPaCT), Orlando, FL, March 2011

17. **X. Han**, J. Bian, E. Y. Sidky, and X. Pan, "Feasibility study of low-dose intra-operative cone-beam CT for image-guided surgery," SPIE Medical Imaging, Orlando, FL 2011

18. J. Bian, K. Yang, **X. Han**, E. Y. Sidky, J. M. Boone, and X. Pan, "Constrained-Total-Variation-Minimization-Based Image Reconstruction in Breast CT," AAPM, Vancouver, BC, 2011

19. Z. Zhang, **X. Han**, E. Pearson, J. Bian, E. Y. Sidky, C. A. Pelizzari, and X. Pan, "A Preliminary Study on Optimizing Cone-beam CT Image Quality by Choosing Combinations of Dose-allocation Schemes and Image-reconstruction Algorithms," AAPM, Vancouver, BC, 2011

20. **X. Han**, J. Bian, Diane Eaker, Timothy Kline, E. Y. Sidky, E. Ritman, and X. Pan, “Reconstruction of Sparse Images from Few-view Cone-beam Data,” AAPM, Vancouver, BC, 2011

21. Z. Zhang, J. Bian, **X. Han**, E. Pearson, E. Y. Sidky, and X. Pan, “Iterative image reconstruction with variable resolution in CT,” IEEE Medical Imaging Conference, Valencia, Spain, October 2011

22. Z. Zhang, **X. Han**, J. Bian, Joseph J. Manak, E. Y. Sidky, and X. Pan, “Initial experience in image reconstruction from limited-angle C-arm CBCT data,” IEEE Medical Imaging Conference, Valencia, Spain, October 2011

23. J. Bian, J. Wang, **X. Han**, E. Y. Sidky, J. Ye, S. Prevrhal, H. Liang, L. Shao, and X. Pan, “Sparse-view image reconstruction from gated cardiac data,” IEEE Medical Imaging Conference, Valencia, Spain, October 2011

24. J. Bian, **X. Han**, K. Yang, E. Y. Sidky, J. M. Boone, and X. Pan, “A preliminary study of image reconstruction from low-dose data in dedicated breast CT,” IEEE Medical Imaging Conference, Valencia, Spain, October 2011

25. E. Pearson, **X. Han**, X. Pan, and C. A. Pelizzari, “Iterative Reconstruction for Axial Field of View Extension in Radiotherapy Cone-Beam CT,” IEEE Medical Imaging Conference, Valencia, Spain, October 2011

26. **X. Han**, J. Bian, D. R. Eaker, E. Y. Sidky, E. L. Ritman, X. Pan, “An Investigation on Image Reconstruction of Coronary Arteries from Few-View Data,” IEEE Medical Imaging Conference, Valencia, Spain, October 2011

27. **X. Han**, E. Pearson, J. Bian, E. Y. Sidky, C. A. Pelizzari, and X. Pan, “Improving Clinical CBCT Imaging Performance with optimization-based image-reconstruction technique,” RSNA, Chicago, IL, 2011

28. J. Bian, J. Wang, **X. Han**, E. Y. Sidky, L. Shao, and X. Pan, “A Preliminary Study of Optimization-based Image Reconstruction from Offset-Detector CBCT,” Proceedings of the 2nd International Conference on Image Formation in X-ray Computed Tomography, 2012

29. Z. Zhang, J. Bian, **X. Han**, D. Shi, A. Zamyatin, P. Rogalla, E. Y. Sidky, and X. Pan, “Iterative Image Reconstruction with Variable Resolution in Diagnostic CT,” Proceedings of the 2nd International Conference on Image Formation in X-ray Computed Tomography, 2012

30. Z. Zhang, **X. Han**, J. Bian, D. Shi, A. Zamyatin, E. Y. Sidky, and X. Pan, “Initial Experience in Constrained-TV-minimization Image Reconstruction from Diagnostic-CT Data,” Proceedings of the 2nd International Conference on Image Formation in X-ray Computed Tomography, 2012

31. J. Bian, J. Wang, **X. Han**, E. Y. Sidky, L. Shao, and X. Pan, “A Preliminary Investigation of CT-Dose Reduction for SPECT/CBCT Attenuation Correction,” IEEE Medical Imaging Conference, Anaheim, CA, 2012

32. Z. Zhang, J. Bian, **X. Han**, D. Shi, A. Zamyatin, E. Y. Sidky, and X. Pan, "A Preliminary Investigation of Image Reconstruction with Variable Resolution in Diagnostic CT", IEEE Nucl. Sci. Conf. Rec., 2012, M17-22

33. Z. Zhang, **X. Han**, J. Bian, D. Shi, A. Zamyatin, P. Rogalla, E. Sidky, and X. Pan, "Constrained TV-Minimization Image Reconstruction from Sparse-View Diagnostic CT Data", IEEE Nucl. Sci. Conf. Rec., 2012, M17-23

34. J. Bian, J. Wang, **X. Han**, E. Sidky, L. Shao, X. Pan, “TV-Minimization-based Iterative Image Reconstruction With an Offset-Detector CBCT in SPECT/CT,” RSNA, Chicago, IL, 2012

35. **X. Han**, M. Silver, S. Oishi, Z. Zhang, J. Bian, E. Y. Sidky, and X. Pan, “Fully Incorporated Scanning Geometry for Improved Accuracy in C-arm CBCT Image Reconstruction,” AAPM, Charlotte, NC, 2012

36. Z. Zhang, **X. Han**, J. Bian, A. Zamyatin, E. Y. Sidky, and X. Pan, "Investigation of Accurate Image Reconstruction from Truncated, Diagnostic-CT Data", SPIE Medical Imaging, Lake Buena Vista, Florida, 2013

37. **X. Han**, E. Pearson, C. A. Pelizzari, X. Pan, “Investigation of Potential Image Quality Improvement of Clinical CBCT,” Varian Research Partners Symposium, Atlanta, GA, 2013

38. Z. Zhang, **X. Han**, J. Bian, D. Shi, A. Zamyatin, P. Rogalla, E. Y. Sidky, and X. Pan, “Investigation in Constrained-TV-minimization Image Reconstruction from Reduced-view Diagnostic-CT Data,” RSNA, Chicago, IL, 2013 (submitted)

39. Z. Zhang, J. Bian, **X. Han**, D. Shi, A. Zamyatin, E. Y. Sidky, and X. Pan, “Optimization-based Image Reconstruction with Variable Resolution in Diagnostic CT,” RSNA, Chicago, IL, 2013 (submitted)

40. J. Bian, **X. Han**, K. Yang, E. Y. Sidky, J. Boone, X. Pan, “Evaluation of TV-minimization-based reconstruction for low-dose dedicated breast CT,” RSNA, Chicago, IL, 2013 (submitted)

41. J. Bian, **X. Han**, K. Yang, E. Y. Sidky, X. Pan, “Iterative image reconstruction for low-dose dedicated breast CT,” RSNA, Chicago, IL, 2013 (submitted)

42. **X. Han**, S. Oishi, T. Satow, H. Yokomama, M. Yamada, M. Silver, Yu-Bing Chang, E. Y. Sidky, and X. Pan, “Low-dose C-arm CBCT Imaging of Vascular Diseases,” RSNA, Chicago, IL, 2013 (submitted)

43. **X. Han**, S. Oishi, T. Satow, H. Yokomama, M. Yamada, M. Silver, Y. Chang, E. Y. Sidky, and X. Pan, “Artifact-suppressed, Low-dose C-arm CBCT Imaging of Low-contrast Cerebral Lesions,” RSNA, Chicago, IL, 2013 (submitted)

44. **X. Han**, E. Pearson, J. Bian, E. Y. Sidky, C. A. Pelizzari, and X. Pan, “Evaluation of Improved Cone-beam CT Image Quality by Optimization-based Reconstruction Algorithms,” RSNA, Chicago, IL, 2013 (submitted)

CONCLUSIONS

Throughout the three years of research supported by the Training Award, I have investigated and implemented novel scanning trajectories with aid of additional hardware components and software control. Simulation data have been generated for initial test of object coverage for these scanning trajectories. I have also acquired real data of physical phantoms by using a clinical CBCT system under a variety of sampling configurations, including full-view, sparse-view, truncated data, and offset-detector configurations. I carried out a rigorous investigation on developing optimization-based image reconstruction algorithms by specifying a discrete imaging model, formulating optimization programs, and designing and implementing iterative algorithms. I have designed a host of parameters for the imaging model, optimization programs, and iterative algorithms, and strategies for adaptively selecting these parameters have been laid out. I have used developed optimization-based algorithms to reconstruct images from data acquired under various sampling configurations. Prior images have been investigated for incorporation in image reconstruction tasks for all the data acquisition configurations. Physical phantoms, including standardized QA phantom and anthropomorphic phantoms, were scanned with CT and CBCT for evaluation of the algorithms developed. Patient data were collected and used for full- and few-view reconstruction. I have validated, characterized, and assessed the reconstruction quality by using simulation data, physical phantom data, and patient data. Quantitative metrics have been calculated for quantitatively characterizing and evaluating the reconstruction quality, choice of parameters, and strategies for incorporating prior images. I have demonstrated that prior-image-incorporated iterative reconstruction algorithms can potentially enhance high-quality CBCT images for IGRT, and that images such reconstructed from substantially reduced data may still bear high clinical IGRT utility.

In summary, I have achieved the goals planned for the all three years. The techniques developed in the project have high technical significance in that image quality of current CBCT can potentially be improved by the algorithms developed, and that novel, low-dose CBCT imaging can be enabled by the algorithms developed. I have also achieved the training goals of the award. The research of the training lead to numerous publications and conference abstracts. Upon completion of this project, I also successfully earned my PhD degree with a dissertation written on topics closely related to this project.

REFERENCES

1. Cancer Fact and Figures, American Cancer Society, 2010, (http://www.cancer.org/research/cancerfactsfigures/cancerfactsfigures/cancer-facts-and-figures-2010)

2. L. A. Dawson and M. B. Sharpe, “Image-guided radiotherapy: rationale, benefits, and limitations,” Lancet Oncol. 7, 848-858, 2006

3. R. D. Timmerman and L. Xing, “Image-guided and adaptive radiation therapy,” Lippincott Williams & Wilkins, 2009

4. A. A. Martinez, D. Yan, D. Lockman, D. Brabbins, K. Kota, M. Sharpe, D. A. Jaffray, F. Vicini, and J. Wong, “Improvement in dose escalation using the process of adaptive radiotherapy combined with three-dimensional conformal or intensity-modulated beams for prostate cancer”, Int J Radiat Oncol Biol Phys. 2001 Aug 1;50(5):1226-34.

5. C. Vargas, A. A. Martinez, L. L. Kestin, D. Yan, I. Grills, D. S. Brabbins, D. M. Lockman, J. Liang, G. S. Gustafson, P. Y. Chen, F. A. Vicini, and J. W. Wong, “Dose-volume analysis of predictors for chronic rectal toxicity after treatment of prostate canceer with adaptive image-guided radiotherapy”, Int. J. Radiat. Oncol. Biol. Phys. 62, 1297-1308, 2005

6. W. Song and B. Schaly, “Image-guided adaptive radiation therapy (IGART): Radiobiological and dose escalation considerations for localized carcinoma of the prostate”, Med. Phys. 32, 2193-2203, 2005

7. J. Nijkamp, F. J. Pos, T. T. Nuver, R. de Jong, P. Remeijer, J.-J. Sonke, and J. V. Lebesque, “Adaptive Radiotherapy for Prostate Cancer Using Kilovoltage Cone-Beam Computed Tomography: First Clinical Results,” *Int. J. Radiat. Oncol. Biol. Phys.* 70, 75-82, 2008

8. Q. J. Wu, D. Thongphiew, Z. Wang, B. Mathayomchan, V. Chankong, S. Yoo, W. R. Lee, and F.-F. Yin, “On-line re-optimization of prostate IMRT plans for adaptive radiation therapy,” Phys. Med. Biol. 53, 673, 673-691, 2008

9. M. K. Islam, H. Alasti, D. J. Moseley, M. B. Sharpe, T. G. Purdie, B. D. Norrlinger, J. H. Siewerdsen, and D. A. Jaffray, “Patient dose from kilovoltage cone beam computed tomography imaging in radiation therapy,” Med. Phys. 33, 1573-1582, 2006

10. N. Wen, H. Guan, R. Hammoud, D. Pradhan, T. Nurushev, S. Li, and B. Movsas, “Dose delivered from Varian’s CBCT to patients receiving IMRT for prostate cancer,” *Phys. Med. Biol.* 52, 2267-2276, 2007

11. M. W. K. Kan, L. H. T. Leung, W. Wong, and N. Lam, “Radiation Dose From Cone Beam Computed Tomography for Image-Guided Radiation Therapy,” *Int. J. Radiat. Oncol. Biol. Phys.* 70, 272-279, 2008

12. G. X. Ding, D. M. Duggan, and C. W. Coffey, “Accurate patient dosimetry of kilovoltage cone-beam CT in radiation therapy,” *Med. Phys.* 35, 1135-1144, 2008

13. H. K. Tuy, “An inversion formula for cone-beam reconstruction,” *SIAM J. Appl. Math.*, 43, 546-552, 1983

14. Y. Zou, and X. Pan, and E. Y. Sidky, “Theory and algorithms for image reconstruction on chords and within regions of interest”, *J. Opt. Soc. Am. A*, Vol 22, pp. 2372–2384, 2005

15. W. P. Segars, G. Sturgeon, S. Mendonca, J. Grimes, and B. M. W. Tsui, “4D XCAT phantom for multimodality imaging research,” *Med. Phys.* 37(9), 4902-4915, 2010

16. S. Cho, D. Xia, C. A. Pelizzari, and X. Pan, “A BPF-FBP tandem algorithm for image reconstruction in reverse helical cone-beam CT”, *Med. Phys.*, 37(1), 32-39, 2010

17. X. Han, J. Bian, D. R. Eaker, T. L. Kline, E. Y. Sidky, E. L. Ritman, and X. Pan, “Algorithm-enabled low-dose micro-CT imaging,” *IEEE Trans. Med. Imaging*, 30, 606-620, 2011

18. X. Pan, E. Y. Sidky, and M. Vannier, “Why do commercial CT scanners still employ traditional, filtered back-projection for image reconstruction?” *Inverse Probl.*, vol. 25, p. 123009, 2009.

19. X. Han, E. Pearson, J. Bian, S. Cho, E. Y. Sidky, C. A. Pelizzari, and X. Pan, “Preliminary investigation of optimal imaging parameters for dose-reduction in cone-beam CT,” IEEE Medical Imaging Conference, Knoxville, TN, October 2010

20. E. Y. Sidky, C.-M. Kao, and X. Pan, “Accurate image reconstruction from few-views and limited-angle data in divergent-beam CT”, *J. X-ray Sci. Tech.*, Vol. 14, pp. 119–139, 2006.

21. E. Y. Sidky and X. Pan,“Image reconstruction in circular cone-beam computed tomography by constrained, total-variation minimization”, *Phys. Med. and Bio.*, Vol. 53, pp. 4777–4807, 2008.

22. A. Wirgin, “The inverse crime,” *arXiv:math-ph/0401050v1*, 2004

23. `http://www.imp.uni-erlangen.de/phantoms/`

24. J. Bian, J. H. Siewerdsen, X. Han, E. Y. Sidky, J. L. Prince, C. A. Pelizzari, and X. Pan,“Evaluation of sparse-view reconstruction from flat-panel-detector cone-beam CT,” *Physics in Medicine and Biology*, vol. 55, pp 6575-6599, 2010

25. X. Han, S. Shi, J. Bian, P. Helm, E. Y. Sidky, and X. Pan, “Feasibility study of low-dose intra-operative cone-beam CT for image-guided surgery,” Proc. SPIE, 7961, 79615P, 2011

26. Z. Wang and A. Bovik, “A universal image quality index,” *IEEE Signal Process. Lett.*, Vol. 9, pp. 81–84, 2002.

27. X. Han, J. Bian, T. L. Kline, D. R. Eaker, E. Y. Sidky, E. L. Ritman, and X. Pan, “Optimization-based reconstruction of sparse images from few-view projections,” *Physics in Medicine and Biology* vol. 57 (16), 2012

28. J. Bian, J. Wang, X. Han, E. Y. Sidky, J. Ye, S. Prevrhal, H. Liang, L. Shao, and X. Pan, “Sparse-view image reconstruction from gated cardiac data,” IEEE Nucl. Sci. Conf. Rec., 2011

29. J. Bian, J. Wang, X. Han, E. Y. Sidky, L. Shao and X. Pan, “Optimization-based image reconstruction from sparse-view data in offset-detector CBCT,” *Physics in Medicine and Biology* vol. 58 (2), 2013

30. X. Han, “Investigation and Applications of Optimization-Based Image Reconstruction in Full- and Reduced-View Cone-Beam Computed Tomography,” Ph.D. Dissertation, The University of Chicago, 2013

31. X. Han, E. Pearson, E. Y. Sidky, C. A. Pelizzari, and X. Pan, “Algorithm-enabled exploration of image-quality potential in cone-beam CT for image-guided radiation therapy,” *(to be submitted in June, 2013)*